Supplementary Information - Thermal transport by phonons and electrons in aluminum, silver, and gold from first principles

Ankit Jain and Alan J. H. McGaughey*

Department of Mechanical Engineering,

Carnegie Mellon University, Pittsburgh PA 15213

*mcgaughey@cmu.edu

S1. METHOD

S1.1. Electron Transport

The electronic transport properties can be obtained by solving the Boltzmann transport equation (BTE) and using the Onsager relations from:[1]

$$\sigma_{\alpha\beta} = -\frac{e^2 n_s}{V} \sum_{\boldsymbol{\kappa}m} \frac{\partial f_{\boldsymbol{\kappa}m}}{\partial \epsilon} v_{\boldsymbol{\kappa}m,\alpha} v_{\boldsymbol{\kappa}m,\beta} \tau_{\boldsymbol{\kappa}m}, \tag{S1}$$

$$[\sigma S]_{\alpha\beta} = -\frac{e n_s}{VT} \sum_{\boldsymbol{\kappa}m} (\epsilon_{\boldsymbol{\kappa}m} - \mu) \frac{\partial f_{\boldsymbol{\kappa}m}}{\partial \epsilon} v_{\boldsymbol{\kappa}m,\alpha} v_{\boldsymbol{\kappa}m,\beta} \tau_{\boldsymbol{\kappa}m}, \tag{S2}$$

$$K_{\alpha\beta} = -\frac{n_s}{VT} \sum_{\boldsymbol{\kappa}m} (\epsilon_{\boldsymbol{\kappa}m} - \mu)^2 \frac{\partial f_{\boldsymbol{\kappa}m}}{\partial \epsilon} v_{\boldsymbol{\kappa}m,\alpha} v_{\boldsymbol{\kappa}m,\beta} \tau_{\boldsymbol{\kappa}m}, \tag{S3}$$

where $\underline{\boldsymbol{\sigma}}, \underline{\boldsymbol{S}}$, and $\underline{\boldsymbol{K}}$ are 3×3 tensors. $\underline{\boldsymbol{\sigma}}$ is the electrical conductivity, $\underline{\boldsymbol{S}}$ is the Seeback coefficient, and $\underline{\boldsymbol{K}}$ is related to the electronic thermal conductivity, $\underline{\boldsymbol{k}}_e$, through $\underline{\boldsymbol{k}}_e = \underline{\boldsymbol{K}} - \underline{\boldsymbol{S}\boldsymbol{\sigma}\boldsymbol{S}}T$, where T is temperature. The summation in these three equations is over all the electrons enumerated using electronic wave vector $\boldsymbol{\kappa}$ and band index m. e is the elementary charge, n_s is the number of electrons per state (two in this study of non-magnetic metals), V is the crystal volume, $f_{\boldsymbol{\kappa}m}$ is the Fermi-Dirac distribution, $\epsilon_{\boldsymbol{\kappa}m}$ is the electron energy, μ is the chemical potential, $v_{\boldsymbol{\kappa}m,\ alpha}$ is the α-component of the electron velocity, $\boldsymbol{v}_{\boldsymbol{\kappa}m} = \frac{1}{\hbar}\frac{\partial \epsilon_{\boldsymbol{\kappa}m}}{\partial \boldsymbol{\kappa}}$, $\hbar$ is the reduced Planck constant, and $\tau_{\boldsymbol{\kappa}m}$ is the electron transport relaxation time. The electron transport relaxation time, limited by electron-phonon scattering, can be obtained by considering the electron-phonon interactions as[1]

$$\begin{aligned}\frac{1}{\tau_{\boldsymbol{\kappa}m}} = \frac{2\pi}{\hbar} \sum_{\boldsymbol{\kappa}'n} \sum_{\boldsymbol{q}\nu} \left| g^{\nu}_{mn}(\boldsymbol{\kappa}\boldsymbol{\kappa}', \boldsymbol{q}) \right|^2 \Big\{ & \left(n_{\boldsymbol{q}\nu} + f_{\boldsymbol{\kappa}'n}\right) \delta\left(\epsilon_{\boldsymbol{\kappa}m} + \hbar\omega_{\boldsymbol{q}\nu} - \epsilon_{\boldsymbol{\kappa}'n}\right) \delta_{\boldsymbol{\kappa}+\boldsymbol{q}-\boldsymbol{\kappa}'} \\ & + \left(n_{\boldsymbol{q}\nu} + 1 - f_{\boldsymbol{\kappa}'n}\right) \delta\left(\epsilon_{\boldsymbol{\kappa}m} - \hbar\omega_{\boldsymbol{q}\nu} - \epsilon_{\boldsymbol{\kappa}'n}\right) \delta_{\boldsymbol{\kappa}-\boldsymbol{q}-\boldsymbol{\kappa}'} \Big\} \left(1 - \frac{\boldsymbol{v}_{\boldsymbol{\kappa}m} \cdot \boldsymbol{v}_{\boldsymbol{\kappa}'n}}{|\boldsymbol{v}_{\boldsymbol{\kappa}m}||\boldsymbol{v}_{\boldsymbol{\kappa}'n}|}\right).\end{aligned} \tag{S4}$$

Here, $g^{\nu}_{mn}(\boldsymbol{\kappa}\boldsymbol{\kappa}', \boldsymbol{q})$ is the electron-phonon matrix element between states $|\boldsymbol{\kappa}m\rangle$ and $|\boldsymbol{\kappa}'n\rangle$,

$$g^{\nu}_{mn}(\boldsymbol{\kappa}\boldsymbol{\kappa}', \boldsymbol{q}) = \sqrt{\frac{\hbar}{2\omega_{\boldsymbol{q}\nu}}} \left\langle \boldsymbol{\kappa}'n \right| \partial_{\boldsymbol{q}\nu} V \left| \boldsymbol{\kappa}m \right\rangle, \tag{S5}$$

where $\partial_{\boldsymbol{q}\nu} V$ is the derivative of the self-consistent potential with respect to phonon mode $|\boldsymbol{q}\nu\rangle$. $g^{\nu}_{mn}(\boldsymbol{\kappa}\boldsymbol{\kappa}', \boldsymbol{q})$ describes the electron-phonon coupling strength when an electron in state

$|\boldsymbol{\kappa}m\rangle$ is scattered into state $|\boldsymbol{\kappa}^{'}n\rangle$ by a phonon in state $|\boldsymbol{q}\nu\rangle$ of energy $\hbar\omega_{\boldsymbol{q}\nu}$ and occupation $n_{\boldsymbol{q}\nu}$. The delta functions in Eqn. (S4) ensure energy and crystal momentum conservation. $\delta(\epsilon)$ is zero unless $\epsilon = 0$ and $\delta_{\boldsymbol{\kappa}}$ is zero unless $\boldsymbol{\kappa} = \boldsymbol{G}$, where $\boldsymbol{G}$ is a reciprocal lattice vector.

S1.2. Phonon Transport

As given in Eqn. (**??**) in the main text, similar to the electron transport, an expression for the elements of the phonon thermal conductivity tensor can be obtained by solving the BTE and using the Fourier law and is[2,3]

$$k_{p,\alpha\beta} = \sum_{\boldsymbol{q}\nu} c_{\boldsymbol{q}\nu} v_{\boldsymbol{q}\nu,\alpha} v_{\boldsymbol{q}\nu,\beta} \tau_{\boldsymbol{q}\nu}. \tag{S6}$$

The summation in Eqn. (S6) is over all the phonon modes in the first Brillioun zone. On the right-hand side of Eqn. (S6), $c_{\boldsymbol{q}\nu}$ is the volumetric specific heat, $v_{\boldsymbol{q}\nu,\alpha}$ is the α-component of the phonon group velocity vector $\boldsymbol{v}_{\boldsymbol{q}\nu}$, and $\tau_{\boldsymbol{q}\nu}$ is the phonon lifetime. The phonon volumetric specific heat can be obtained by using the Bose-Einstein statistics as $c_{\boldsymbol{q}\nu} = \frac{\hbar\omega_{\boldsymbol{q}\nu}}{V}\frac{\partial n^o_{\boldsymbol{q}\nu}}{\partial T}$, where $n^o_{\boldsymbol{q}\nu}$ is the Bose-Einstein distribution. The group velocity vector is related to the mode frequency as $\boldsymbol{v}_{\boldsymbol{q}\nu} = \frac{\partial\omega_{\boldsymbol{q}\nu}}{\partial\boldsymbol{q}}$. Under the commonly-used relaxation time approximation (RTA) of the BTE, the phonon lifetime can be estimated using the inverse of the phonon scattering rate, $\frac{partialn_{\boldsymbol{q}\nu}}{\partial t}$.[2,4,5]

Harmonic lattice dynamics calculations can be used to obtain the phonon frequencies.[6] The dynamical matrix, $\mathbf{D}(\boldsymbol{q})$, has elements

$$D^{\alpha\alpha^{'}}_{\tau\tau^{'}}(\boldsymbol{q}) = \sum_{\mathbf{R}^{'}} \frac{1}{\sqrt{m_\tau m_{\tau^{'}}}} \Phi^{\alpha\alpha^{'}}_{\mathbf{0}\tau,\mathbf{R}^{'}\tau^{'}} \exp(\mathrm{i}\boldsymbol{q}\cdot\mathbf{R}^{'}). \tag{S7}$$

Here, the summation is over all unit cells, which are located at position vector $\mathbf{R}^{'}$, and m_τ is the mass of atom τ in the unit cell. $\Phi^{\alpha\alpha^{'}}_{\mathbf{0}\tau,\mathbf{R}^{'}\tau^{'}}$ is the second-order (i.e., harmonic) force constant linking the motions of atom ($\mathbf{0}$, τ) (atom τ in the unit cell at $\mathbf{0}$) in the α-direction and atom ($\mathbf{R}^{'}, \tau^{'}$) in the $\alpha^{'}$-direction. The phonon frequencies and eigenvectors, $\mathbf{e}_{\boldsymbol{q}\nu}$, can then be obtained by solving the eigenvalue problem

$$(\omega_{\boldsymbol{q}\nu})^2 \mathbf{e}_{\boldsymbol{q}\nu} = \mathbf{D}(\boldsymbol{q})\mathbf{e}_{\boldsymbol{q}\nu}. \tag{S8}$$

We consider phonon-phonon and phonon-electron interactions. The phonon scattering rates due to three-phonon scattering are calculated using the RTA solution of the BTE from[2,5]

$$\frac{1}{\tau^{pp}_{\boldsymbol{q}\nu}} = \frac{\pi\hbar}{16N}\sum_{\boldsymbol{q}'\nu'}\sum_{\boldsymbol{q}''\nu''}\left|V^{\boldsymbol{q}\boldsymbol{q}'\boldsymbol{q}''}_{\nu\nu'\nu''}\right|^2\Big\{(n^o_{\boldsymbol{q}'\nu'}+n^o_{\boldsymbol{q}''\nu''}+1)\delta(\omega_{\boldsymbol{q}\nu}-\omega_{\boldsymbol{q}'\nu'}-\omega_{\boldsymbol{q}''\nu''})+(n^o_{\boldsymbol{q}'\nu'}-n^o_{\boldsymbol{q}''\nu''}) \times\left[\delta(\omega_{\boldsymbol{q}\nu}+\omega_{\boldsymbol{q}'\nu'}-\omega_{\boldsymbol{q}''\nu''})-\delta(\omega_{\boldsymbol{q}\nu}-\omega_{\boldsymbol{q}'\nu'}+\omega_{\boldsymbol{q}''\nu''})\right]\Big\}, \tag{S9}$$

where N is the total number of phonon modes. $V^{\boldsymbol{q}\boldsymbol{q}'\boldsymbol{q}''}_{\nu\nu'\nu''}$ is the three-phonon scattering matrix element, which depends on the third-order force constants $\Phi^{\alpha\alpha'\alpha''}_{0\tau,\mathbf{R}'\tau'',\mathbf{R}''\tau''}$ and is defined as

$$V^{\boldsymbol{q}\boldsymbol{q}'\boldsymbol{q}''}_{\nu\nu'\nu''} = \sum_{\mathbf{R}''\tau''\alpha''}\sum_{\mathbf{R}'\tau'\alpha'}\sum_{\tau\alpha}\delta_{\boldsymbol{q}+\boldsymbol{q}'+\boldsymbol{q}''}\;\Phi^{\alpha\alpha'\alpha''}_{0\tau,\mathbf{R}'\tau'',\mathbf{R}''\tau''} \times\frac{e^{\mathrm{i}(\boldsymbol{q}'\cdot\mathbf{R}'+\boldsymbol{q}''\cdot\mathbf{R}'')}e^{\tau\alpha}_{\boldsymbol{q}\nu}e^{\tau'\alpha'}_{\boldsymbol{q}'\nu'}e^{\tau''\alpha''}_{\boldsymbol{q}''\nu''}}{\sqrt{m_\tau m_{\tau'}m_{\tau''}\omega_{\boldsymbol{q}\nu}\omega_{\boldsymbol{q}'\nu'}\omega_{\boldsymbol{q}''\nu''}}}, \tag{S10}$$

where $e^{\tau\alpha}_{\boldsymbol{q}\nu}$ is the α-component of the eigenvector $\mathbf{e}_{\boldsymbol{q}\nu}$ for atom τ.

The phonon-electron scattering rate for the phonon mode $\boldsymbol{q}\nu$ is[1]

$$\frac{1}{\tau^{ep}_{\boldsymbol{q}\nu}} = \frac{2\pi}{\hbar}\sum_{\boldsymbol{\kappa}mn}w_{\boldsymbol{\kappa}}\left|g^{\nu}_{mn}(\boldsymbol{\kappa}\boldsymbol{\kappa}',\boldsymbol{q})\right|^2\left(f_{\boldsymbol{\kappa}m}-f_{\boldsymbol{\kappa}'n}\right) \times\delta\left(\epsilon_{\boldsymbol{\kappa}m}+\hbar\omega_{\boldsymbol{q}\nu}-\epsilon_{\boldsymbol{\kappa}'n}\right), \tag{S11}$$

where $w_{\boldsymbol{\kappa}}$ is the weight of the $\boldsymbol{\kappa}$-point normalized to two for non-magnetic calculations and $\boldsymbol{\kappa}' = \boldsymbol{\kappa}+\boldsymbol{q}$. The phonon-phonon and phonon-electron relaxation times are combined using the Matthiessen rule[7] to obtain the effective lifetime of phonon mode $\boldsymbol{q}\nu$,

$$\frac{1}{\tau_{\boldsymbol{q}\nu}} = \frac{1}{\tau^{pp}_{\boldsymbol{q}\nu}}+\frac{1}{\tau^{ep}_{\boldsymbol{q}\nu}}. \tag{S12}$$

S2. SIMULATION PARAMETERS

For the electron transport property calculations, we calculate the electron Hamiltonian, the phonon dynamical matrix, and the electron-phonon coupling coefficients on coarse $18\times18\times18$ electron and $6\times6\times6$ phonon wave vector grids using density functional theory (DFT)

TABLE S1. DFT simulation parameters for metals.

Metal	Number of valence electrons considered	Relaxed lattice constant using QE (Å)	Plane wave energy cutoff for electron-phonon calculations using QE (eV)	Electronic wave vector grid for integration of charge density over the Brillioun zone	plane wave energy cutoff for force calculations using VASP (eV)	Number of MLWFs for interpolation using Wannier functions
Al	3	3.984	952	$14 \times 14 \times 14$	240	4
Ag	11	4.074	1224	$12 \times 12 \times 12$	250	6
Au	11	4.082	1360	$12 \times 12 \times 12$	230	6

and density functional perturbation theory (DFPT) calculations as implemented in Quantum Espresso (QE)[8]. The electron wave vector grid and the plane wave energy cutoffs used in the integration of the Brillioun zone for constructing the charge density and dynamical matrices are reported in the Table S1. We used a Gaussian smearing of 1.36 eV to obtain better convergence with the number of electronic k-points. After obtaining the required properties on coarse grids, we used the Electron-Phonon Wannier (EPW) package to first calculate maximally localized Wannier functions (MLWF) and then to do the interpolation of the required properties to $80 \times 80 \times 80$ electron and $32 \times 32 \times 32$ phonon wave vector grids using Wannier functions. The number of Wannier functions employed for the three metals are reported in Table S1. We used a smearing of 30 meV to satisfy the energy conservation delta functions in the electron-phonon scattering rate calculations [Eqns. (S4) and (S11)].

For the phonon-phonon scattering rate calculations, the interatomic force constants are obtained using finite differencing of the Hellmann-Feynman forces obtained on a 216 atom supercell with one or two atoms displaced from their equilibrium position by 0.01 Å using the DFT package VASP. We used a $3 \times 3 \times 3$ electronic wave vector grid and a first-order Methfessel-Paxton smearing of 0.1 eV. The plane wave energy cutoffs used are reported in Table S1. The convergence of phonon properties with respect to supercell size and electron k-point sampling was tested thoroughly by Grabowski et al.[9] We used a third nearest-neighbor interaction cutoff for the cubic force constants and we satisfy translational invariance using

a Lagrangian approach.[10] The energy conservation delta functions in the phonon-phonon scattering rate calculations [Eqn. (S9)] are satisfied using the adaptive broadening approach discussed by Turney et al.[4]

We performed non-spin calculations using the local density approximation (LDA) exchange-correlation based norm-conserving and projected augmented wave pseudopotentials in QE and VASP. The relaxed lattice structure obtained using QE (lattice constants reported in Table S1) is used for the force constant calculation in VASP. We note that since we are using the QE relaxed structure in the VASP force calculation, the extracted force constants do not correspond to zero-pressure. The difference in the relaxed lattice constants from QE and VASP is less than 1%. From our previous study on how strain affects the thermal conductivity of soft and hard materials,[11] we expect the effect of 1% strain on the phonon thermal conductivity to be within the numerical uncertainties (11%). We used VASP for the supercell force calculations because we were unable to get forces from QE on 216 atom supercells with a $3 \times 3 \times 3$ electronic wave vector grid with our computational resources.

S3. VARIATION OF TRANSPORT PROPERTIES WITH SIMULATION PARAMETERS

We performed convergence studies of the phonon and electron transport properties with the simulation parameters for all three metals. We found that the Au transport properties were the most sensitive. All the results plotted in this section are therefore for Au.

S3.1. Cubic force constant cutoff

We first plot the phonon thermal conductivity of Au as a function of temperature by considering different cubic force constant cutoffs in Fig. S1. The cubic force constant interaction cutoff affects only the phonon-phonon scattering rates and as such we plot the thermal conductivities obtained by considering only phonon-phonon interactions. As can be seen from Fig. S1, the phonon thermal conductivity of Au remains unaffected (changes less than 3%) in increasing the cubic force constant cutoff from second to third nearest neighbors. For the other metals, we also find that the thermal conductivity difference for

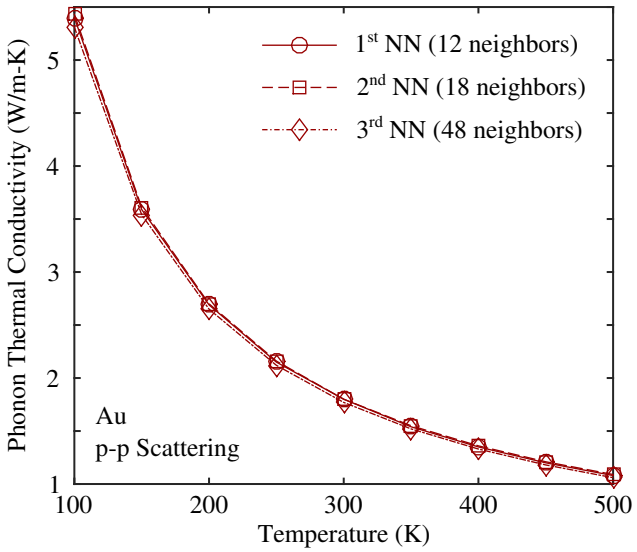

FIG. S1. Phonon thermal conductivity of Au versus temperature for different cubic force constant interaction cutoffs. The phonon thermal conductivity is obtained by considering only the phonon-phonon scattering in this plot. NN and p-p denote nearest neighbors and phonon-phonon.

including up to second and third nearest neighbors is within the numerical uncertainties. Therefore, we include up to third nearest-neighbors interaction in our thermal conductivity calculations for all metals.

S3.2. Phonon wave vector grid

The phonon thermal conductivity variation of Au as a function of the phonon wave vector grid at a temperature of 300 K is plotted in Fig. S2. The phonon thermal conductivities in this plot are obtained by considering only phonon-phonon interactions. The dashed lines in the figure denote $\pm 1\%$ variation from the thermal conductivity corresponding to the maximum phonon wave vector grid considered. As can be seen from Fig. S2, the phonon thermal conductivity is converged to within 1% for an increase in the grid size beyond $26 \times 26 \times 26$. For the other metals, we also found the $26 \times 26 \times 26$ phonon wave vector grid to be converged within 1% for phonon thermal conductivity. As will be shown in Sec. S3.5, however, for the electron transport properties calculations, which require electron-phonon interactions, we need a finer phonon wave vector grids than $26 \times 26 \times 26$ ($32 \times 32 \times 32$). As

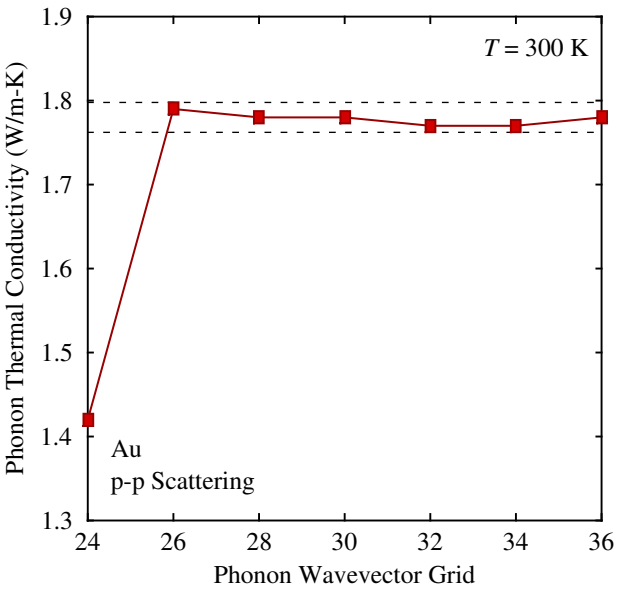

FIG. S2. Phonon thermal conductivity variation with phonon wave vector grid for Au at a temperature of 300 K. The phonon thermal conductivity is obtained by considering only the phonon-phonon scattering in this plot. The dashed black-lines represent a $\pm 1\%$ variation from the $36 \times 36 \times 36$ phonon thermal conductivity. p-p denotes phonon-phonon.

such, we used a $32 \times 32 \times 32$ phonon wave vector grid for the phonon thermal conductivity calculations as well.

S3.3. Coarse electronic wave vector grid

To determine the converged coarse electronic grid, we first calculated the Fermi energy. The results are reported in Table S2. We note that the Fermi energies reported in Table S2 are obtained directly from the DFT calculations without the need for Wannier functions. As can be seen from Table S2, the Fermi energy converges to within 0.0001 eV for electronic wave vector grids larger than $18 \times 18 \times 18$ for all metals and, therefore, an $18 \times 18 \times 18$ coarse electronic wave vector grid is used in this study.

TABLE S2. Fermi energy variation with coarse electronic wave vector grid. A 0.0001 eV convergence is obtained for Al, Ag, and Au for an $18 \times 18 \times 18$ electronic wave vector grid.

Coarse Electronic Grid	Fermi Energy (eV)		
	Al	Ag	Au
6	8.1644	13.4523	15.9755
8	8.0881	13.4310	15.9427
10	8.1197	13.4372	15.9389
12	8.1112	13.4402	15.9386
14	8.1121	13.4409	15.9385
16	8.1123	13.4410	15.9385
18	8.1122	13.4410	15.9385
20	8.1122	13.4410	15.9385
22	8.1122	13.4410	15.9385
24	8.1122	13.4410	15.9385

S3.4. Coarse phonon wave vector grid

To further check the convergence of the coarse electronic wave vector grid and to get the converged coarse phonon wave vector grid, we plot the spatial decay of the Hamiltonian, the phonon dynamical matrix, and the electron-phonon coupling matrix elements in the Wannier functions representation for Au in Figs. S3(a)- S3(d). All of these quantities should decay to zero in order to have the localized Wannier functions that are necessary for high-quality interpolation. As can be seen from Fig. S3, all of these quantities decay very quickly with distance, suggesting the sufficiency of the selected coarse electronic and phonon wave vector grids for interpolation.

S3.5. Fine phonon wave vector grid and energy delta functions for electron-phonon interactions

The variations of the electrical conductivity and electron thermal conductivity of Au at a temperature of 300 K with the fine phonon wave vector grid and the smearing amount for

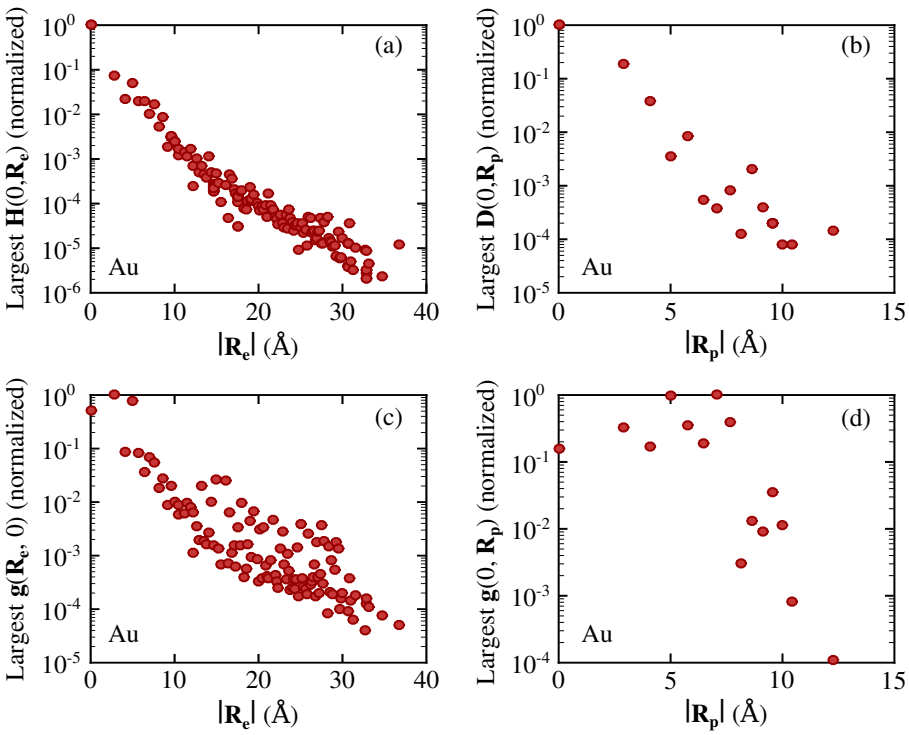

FIG. S3. Spatial decay of the largest component of the (a) Hamiltonian, $\mathbf{H}(0, \mathbf{R_e})$, (b) dynamical matrix, $\mathbf{D}(0, \mathbf{R_p})$, (c) electron-phonon coupling matrix element, $\mathbf{g}(\mathbf{R_e}, 0)$, and (d) $\mathbf{g}(0, \mathbf{R_p})$ for Au. The data are normalized against their largest values and are plotted as a function of position of the electron unit-cell, $\mathbf{R_e}$, or the phonon unit-cell, $\mathbf{R_p}$, used for describing electrons and phonons in the real space.

satisfying the energy conservation delta functions are plotted in Figs. S4(a) and S4(b). A fine electronic wave vector grid of $80 \times 80 \times 80$ k-points is used for all of these results. For Fig. S4(a), a smearing of 30 meV is used to satisfy the delta functions and for Fig. S4(b), a fine phonon wave vector grid of $32 \times 32 \times 32$ q-points is used. The variation in both the electrical conductivity and the electron thermal conductivity is less than 5% in varying the fine phonon wave vector grid from $24 \times 24 \times 24$ to $40 \times 40 \times 40$ and in varying the smearing amount from 3 to 50 meV. We used a fine phonon wave vector grid of $32 \times 32 \times 32$ and a smearing of 30 meV in all of our converged calculations.

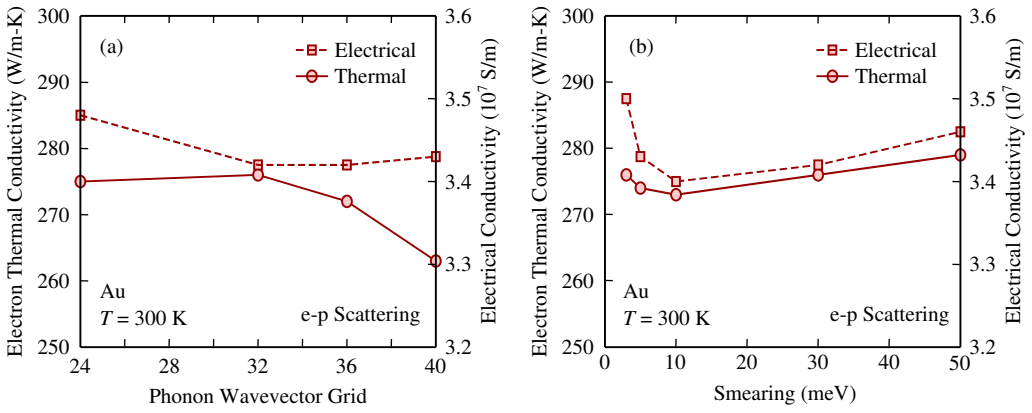

FIG. S4. Variations of the electrical conductivity and electron thermal conductivity of Au at a temperature of 300 K with the (a) phonon wave vector grid and (b) smearing used to satisfy the energy delta functions. e-p represents electron-phonon.

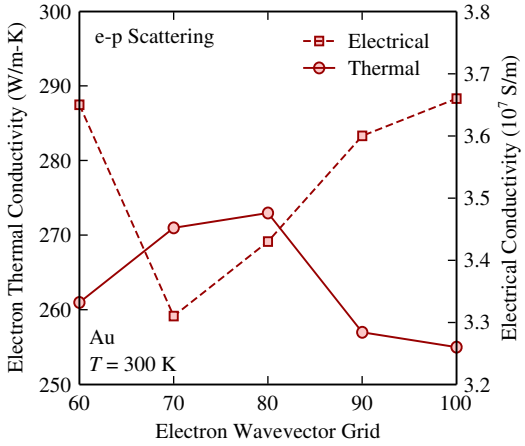

FIG. S5. Variations of the electrical conductivity and electron thermal conductivity of Au at a temperature of 300 K with the fine electron wave vector grid. e-p represents electron-phonon.

S3.6. Fine electron wave vector grid

The variations of the electrical conductivity and electron thermal conductivity of Au at temperature of 300 K with the fine electron wave vector grid are plotted in Fig. S5. A fine phonon wave vector grid of $36 \times 36 \times 36$ and a smearing of 30 meV are used for all of the results in this plot. Varying the fine electronic wave vector grid around $80 \times 80 \times 80$ from $60 \times 60 \times 60$ to $100 \times 100 \times 100$ results in changes in both the electrical conductivity

and electron thermal conductivity of less than 11%. We note that among all the simulation parameters, we found the electron transport properties to be most sensitive to the fine electron wave vector grid. For all the metals considered, the minimum variation is seen in Al (less than 2%). For Ag, the variation is within 10% in changing the grid from $70 \times 70 \times 70$ to $80 \times 80 \times 80$. We used a fine electronic wave vector grid of $80 \times 80 \times 80$ in all of our converged calculations.

S4. HEAT CAPACITY

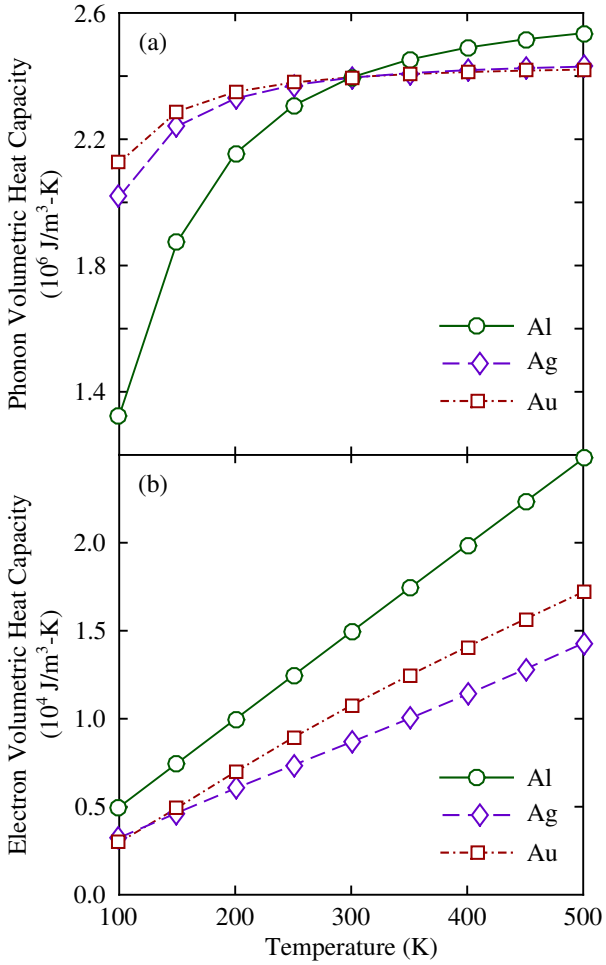

FIG. S6. (a) Phonon and (b) electron volumetric heat capacity variation of Al, Ag, and Au with temperature.

The contributions of phonons and electrons towards the heat capacities can be calculated

from the mode-level properties as:

$$C_p = \frac{1}{V}\sum_{\boldsymbol{q}\nu} \hbar\omega_{\boldsymbol{q}\nu}\frac{\partial n^o_{\boldsymbol{q}\nu}}{\partial T}, \tag{S13}$$

$$C_e = -\frac{n_s}{VT}\sum_{\boldsymbol{\kappa}m}(\epsilon_{\boldsymbol{\kappa}m}-\mu)^2\frac{\partial f_{\boldsymbol{\kappa}m}}{\partial \epsilon}. \tag{S14}$$

The contribution of phonons and electrons towards the volumetric heat capacity of Al, Ag, and Au are plotted in Figs. S6(a) and S6(b). As can be seen from Fig. S6(a), the phonon contribution initially increases with an increase in temperature at lower temperatures and then plateaus to the Dulong-Petit limit at higher temperatures. The electron contribution towards the heat capacity [Fig. S6(b)], on the other hand, increases linearly with an increase in the temperature. For the entire temperature range, the electron contribution towards the heat capacity is less than 1% for all three metals.

S5. ELECTRON THERMAL CONDUCTIVITY AND ELECTRICAL CONDUCTIVITY

The temperature variation of the electron thermal conductivity (k_e) for the three metals is plotted in Fig. S7(a). Amongst the three metals, k_e is highest for Ag followed by Au and Al at all temperatures. Al and Au show increasing k_e with increasing temperature, followed by a maximum, a decrease, and a plateau. The peak is not seen in Ag due to the temperature range considered. The origin of the peak followed by a plateau is the competing effects of increasing electron specific heat (Fig. S6) and decreasing electron lifetimes (due to increased e-p scattering) with increasing temperature. We note that this peak in k_e is different from the more-pronounced experimentally-observed peak at a temperature near 10 K. The origin of that peak is the competing effects of electron specific heat and electron-impurity scattering at very low temperatures. Because we do not consider electron-impurity scattering, we restricted our k_e prediction to intermediate temperatures.

The electrical conductivity variations of Al, Ag, and Au with temperature are plotted in Fig. S7(b). As opposed to the electron thermal conductivities [see Fig. S7(a)], the electrical conductivities do not depend on the heat capacity [Eqn. (S1)] and follow the electron lifetime trend, thus decreasing monotonically with an increase in the temperature.

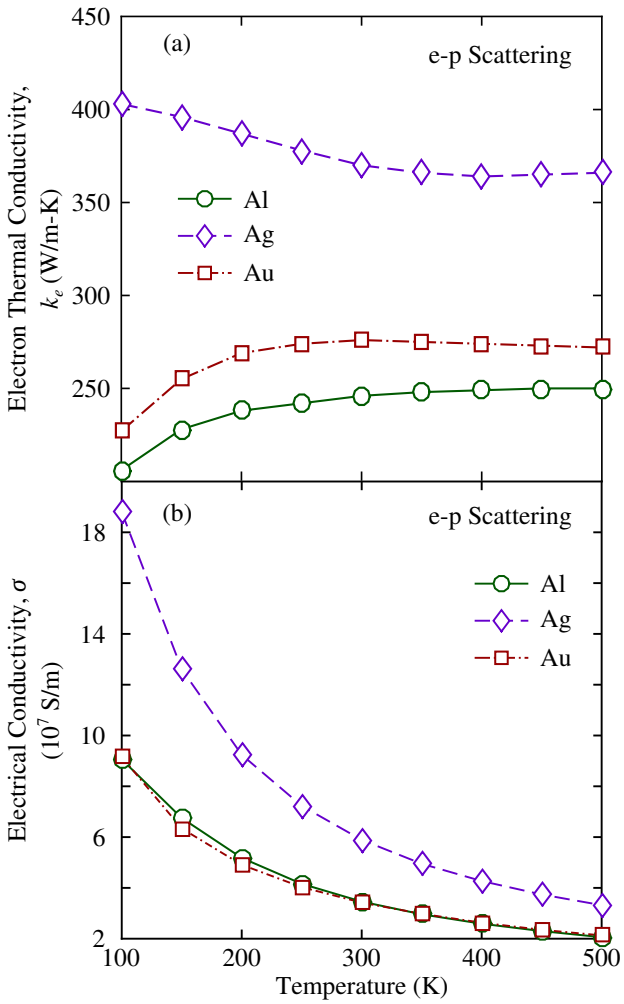

FIG. S7. Variation of (a) electron thermal conductivity, k_e and (b) electrical conductivity, σ, with temperature for Al, Ag, and Au.

S6. ACCUMULATION AND MEAN FREE PATH

The electron and phonon thermal conductivities can be re-written using the electron and phonon mean free paths, $\Lambda_{\boldsymbol{\kappa}m}$ and $\Lambda_{\boldsymbol{q}\nu}$, as

$$K_{\alpha\beta} = -\frac{n_s}{VT}\sum_{\boldsymbol{\kappa}m}(\epsilon_{\boldsymbol{\kappa}m}-\mu)^2\frac{\partial f_{\boldsymbol{\kappa}m}}{\partial\epsilon}\frac{v_{\boldsymbol{\kappa}m,\alpha}v_{\boldsymbol{\kappa}m,\beta}}{|\boldsymbol{v}_{\boldsymbol{\kappa}m}|}\Lambda_{\boldsymbol{\kappa}m}, \tag{S15}$$

$$k_{p,\alpha\beta} = \sum_{\boldsymbol{q}\nu} c_{\boldsymbol{q}\nu}\frac{v_{\boldsymbol{q}\nu,\alpha}v_{\boldsymbol{q}\nu,\beta}}{|\boldsymbol{v}_{\boldsymbol{q}\nu}|}\Lambda_{\boldsymbol{q}\nu}, \tag{S16}$$

where $\Lambda_{\boldsymbol{\kappa}m} = |\boldsymbol{v}_{\boldsymbol{\kappa}m}|\,\tau_{\boldsymbol{\kappa}m}$ and $\Lambda_{\boldsymbol{q}\nu} = |\boldsymbol{v}_{\boldsymbol{q}\nu}|\,\tau_{\boldsymbol{q}\nu}$. The mean free path of a carrier is a measure of the distance it travels between scattering events. The electron and phonon thermal

conductivity accumulations can then be obtained using these definitions of the electron and phonon thermal conductivities as

$$K_{\alpha\beta}(\Lambda) = -\frac{n_s}{VT}\sum_{\boldsymbol{\kappa}m}^{\Lambda_{\boldsymbol{\kappa}m}<\Lambda}(\epsilon_{\boldsymbol{\kappa}m}-\mu)^2\frac{\partial f_{\boldsymbol{\kappa}m}}{\partial\epsilon}\frac{v_{\boldsymbol{\kappa}m,\alpha}v_{\boldsymbol{\kappa}m,\beta}}{|\boldsymbol{v}_{\boldsymbol{\kappa}m}|}\Lambda_{\boldsymbol{\kappa}m}, \tag{S17}$$

$$k_{p,\alpha\beta}(\Lambda) = \sum_{\boldsymbol{q}\nu}^{\Lambda_{\boldsymbol{q}\nu}<\Lambda} c_{\boldsymbol{q}\nu}\frac{v_{\boldsymbol{q}\nu,\alpha}v_{\boldsymbol{q}\nu,\beta}}{|\boldsymbol{v}_{\boldsymbol{q}\nu}|}\Lambda_{\boldsymbol{q}\nu}. \tag{S18}$$

These accumulation functions are plotted and discussed in the main text in Figs. **??**(a) and **??**(b) for Al, Ag, and Au at a temperature of 300 K.

S7. THIN FILMS

Eqns. (S1)-(S3) and (S6) can be used to predict the thermal conductivity of a thin film of thickness L in the cross-plane direction (z direction, i.e., $\alpha, \beta = z$) by including the scattering of electrons and phonons from boundaries using the Matthiessen rule as[7]

$$\frac{1}{\tau^{eff}_{\boldsymbol{\kappa}m}} = \frac{1}{\tau_{\boldsymbol{\kappa}m}} + \frac{|v_{\boldsymbol{\kappa}m,z}|}{L/2}, \tag{S19}$$

$$\frac{1}{\tau^{eff}_{\boldsymbol{q}\nu}} = \frac{1}{\tau_{\boldsymbol{q}\nu}} + \frac{|v_{\boldsymbol{q}\nu,z}|}{L/2}, \tag{S20}$$

where $\tau^{eff}_{\boldsymbol{\kappa}m}$ and $\tau^{eff}_{\boldsymbol{q}\nu}$ are the effective electron and phonon lifetimes. Eqns. (S19) and (S20) are based on the assumptions of uniform electron and phonon distribution functions across the film thickness and diffuse scattering of electrons and phonons at the boundaries.

The phonon and electron thermal conductivity variations for Al, Ag, and Au with film thickness at a temperature of 100 K and 300 K are plotted in Figs. S8(a) and S8(b). Both the phonon and electron thermal conductivities increase with an increase in film thickness due to reduced boundary scattering. As can be seen from Fig. S8(b), the electron thermal conductivity in the bulk metals is highest for Ag followed by Au and Al. For the 50 nm thick films, however, because of smaller electron mean free paths in Al, the electron thermal conductivity is highest for Al followed by Ag and then Au. For 50 nm thick films, the phonon contribution towards the total thermal conductivity is 15%, 13%, and 9% for Al, Ag, and Au at a temperature of 100 K. The phonon contribution reduces with increase in film thickness to 5.5%, 2.5%, and 2.0% for Al, Ag, and Au for the bulk materials at a temperature of 100 K.

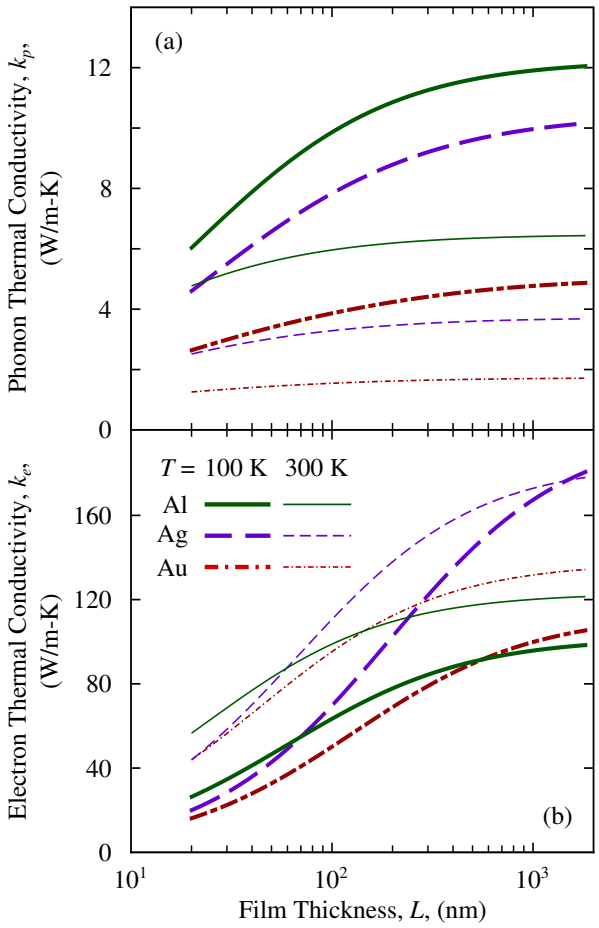

FIG. S8. (a) Phonon and (b) electron thermal conductivity variation of Al, Ag, and Au with film thickness.

S8. SILICON SIMULATION PARAMETERS

We considered isotopically pure silicon. The harmonic force constants are obtained using DFPT calculations. The cubic force constants for the phonon-phonon scattering rate calculations are obtained using a finite differencing of the Hellmann-Feynman forces obtained on a 216 atom supercell with one or two atoms displaced from their equilibrium position by 0.02 Å using QE. We a used $8\times8\times8$ electronic wave vector grid, a 816 eV plane wave energy cutoff, and the LDA exchange-correlation based norm-conserving pseudopotential generated using the Von Barth-Car method.[12] The harmonic force constants are initially obtained on a $8 \times 8 \times 8$ phonon wave vector grid and are later interpolated to a $32 \times 32 \times 32$ grid for phonon scattering rate calculations. Further details regarding convergence can be found in

Ref. 13.

S9. ALUMINUM AND SILICON

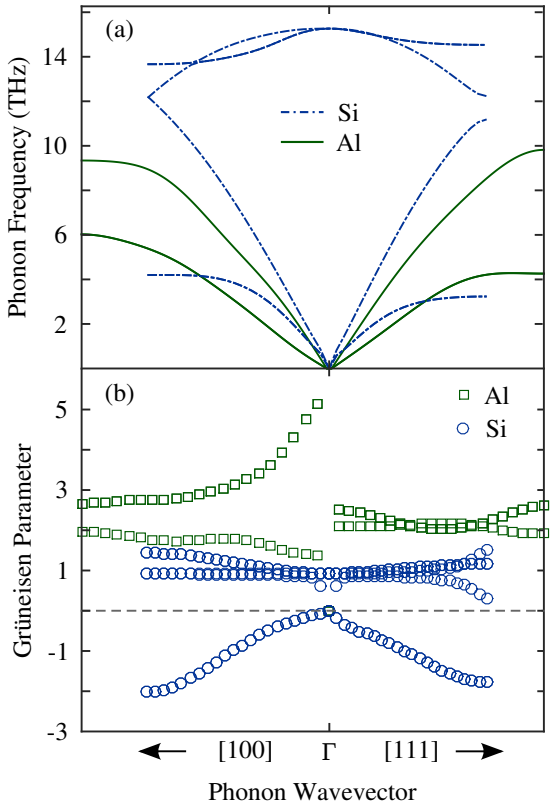

FIG. S9. (a) Phonon dispersions and (b) Grüneisen parameters of Al and Si along the [100] and [111] directions of the first Brillioun zone.

The phonon dispersions of Al and Si along the [100] and [111] directions of the first Brillouin zone are plotted in Fig. S9(a). Both Al and Si have face-centered cubic structure with one and two atoms in the primitive unit-cell. For Al and Si, the [100] group velocities for the transverse (longitudinal) acoustic phonons are 2800 (6800) m/s and 4700 (7600) m/s.

Mode-dependent Grüneisen parameters along [100] and [111] directions for Al and Si are plotted in Fig. S9(b). The Grüneisen parameter is a measure of the anharmonicity of a mode. We calculated the Grüneisen parameters with the cubic force constants by using Eqn. (2) of Ref. 14. As can be seen from Fig. S9(b), the Grüneisen parameters for Al are significantly higher than those for Si, suggesting higher anharmonicity of Al. We characterize

the anharmonicity of Al and Si by calculating an average Grüneisen parameter, γ, as a heat-capacity weighted average of the absolute values of the mode-dependent Grüneisen parameters as:

$$\gamma \equiv \frac{\sum_i c_{ph,i}|\gamma_i|}{\sum_i c_{ph,i}}. \tag{S21}$$

While γ is 1.02 for Si, it is 2.21 for Al at a temperature of 300 K; thus indicating higher anharmonicity and hence lower phonon lifetimes in Al.

S10. ELECTRON-PHONON COUPLING

The rate of energy exchange between electrons at a temperature T_e and phonons at a temperature T_p is[15]

$$\frac{\partial E^{e-p}}{\partial t} = \frac{4\pi}{\hbar}\sum_{\boldsymbol{\kappa}mn}\sum_{\boldsymbol{q}\nu}\hbar\omega_{\boldsymbol{q}\nu}\left|g^{\nu}_{mn}(\boldsymbol{k}\boldsymbol{k}',\boldsymbol{q})\right|^2\left[(f_{\boldsymbol{\kappa}m}-f_{\boldsymbol{\kappa}'n})n_{\boldsymbol{q}\nu}-f_{\boldsymbol{\kappa}'n}(1-f_{\boldsymbol{\kappa}m})\right] \times\delta\left(\epsilon_{\boldsymbol{\kappa}m}+\hbar\omega_{\boldsymbol{q}\nu}-\epsilon_{\boldsymbol{\kappa}'n}\right), \tag{S22}$$

where f and n are evaluated at T_e and T_p, and $\boldsymbol{\kappa}' = \boldsymbol{\kappa}+\boldsymbol{q}$.

The electron-phonon mass enhancement parameter, λ, is a measure of the electron-phonon coupling strength and is defined as[1,16]

$$\lambda = \frac{1}{N}\sum_{\boldsymbol{q}\nu}\frac{1}{N_F\omega_{\boldsymbol{q}\nu}}\sum_{\kappa mn} w_{\boldsymbol{\kappa}}\left|g^{\nu}_{mn}(\boldsymbol{\kappa}\boldsymbol{\kappa}',\boldsymbol{q})\right|^2\delta\left(\epsilon_{\boldsymbol{\kappa}n}\right)\delta\left(\epsilon_{\boldsymbol{\kappa}'m}\right), \tag{S23}$$

where N_f is the density of states at the Fermi level and $\boldsymbol{\kappa}' = \boldsymbol{\kappa}+\boldsymbol{q}$.

Our predicted values of λ are 0.49, 0.16, and 0.18 for Al, Ag, and Au at a temperature of 300 K. These values match well with the suggested values of 0.43 ± 0.05, 0.13 ± 0.04, and 0.17 ± 0.05 for Al, Ag, and Au in literature.[17]

The variations of the electron-phonon coupling factors, G [Eqn. (**??**)], with T_e, T_p, and phonon frequency for Al, Ag, and Au are plotted in Fig. S10, the inset of Fig. S10, and Fig. S11.

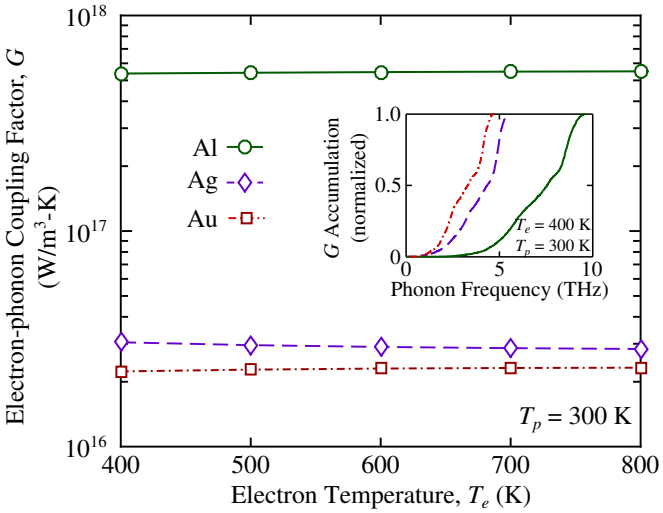

FIG. S10. Variation of e-p coupling factor, G, with electronic temperature, T_e, at a phonon temperature, T_p, of 300 K for Al, Ag, and Au. Accumulations of G with phonon frequency at T_e = 400 K and T_p = 300 K for Al, Ag, and Au are shown in the inset.

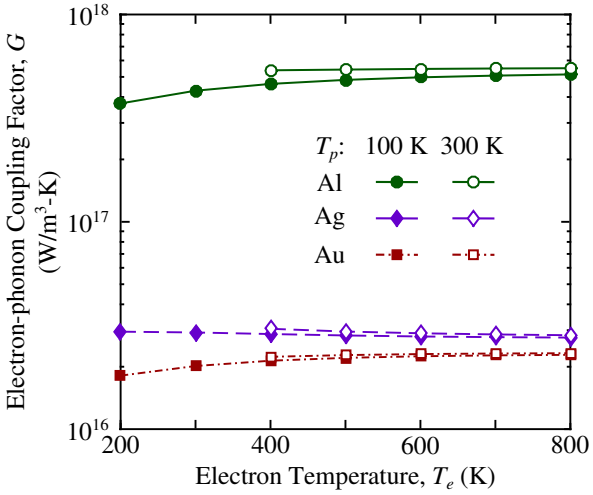

FIG. S11. Variation of the electron-phonon coupling factor, G, with electron temperature, T_e for Al, Ag, and Au at phonon temperatures, T_p, of 100 K and 300 K.

[1] G. D. Mahan, *Many-particle physics* (Springer Science & Business Media, 2013).

[2] J. A. Reissland, *The Physics of Phonons* (John Wiley and Sons Ltd, 1973).

[3] L. Lindsay, D. A. Broido, and T. L. Reinecke, "doibase-10.1103/PhysRevB.87.165201 Phys Rev B **87**, 165201 (2013).

[4] J. E. Turney, E. S. Landry, A. J. H. McGaughey, and C. H. Amon, Physical Review B **79**, 064301 (2009).

[5] D. C. Wallace, *Thermodynamics of Crystals* (Cambridge Univ. Press, Cambridge, UK, 1972).

[6] M. T. Dove, *Introduction to Lattice Dynamics* (Cambridge, Cambridge, 1993).

[7] J. M. Ziman, *Electrons and Phonons* (Oxford University Press, Clarendon, Oxford, 1960).

[8] P. Giannozzi, S. Baroni, N. Bonini, M. Calandra, R. Car, C. Cavazzoni, D. Ceresoli, G. L. Chiarotti, M. Cococcioni, I. Dabo, A. D. Corso, S. de Gironcoli, S. Fabris, G. Fratesi, R. Gebauer, U. Gerstmann, C. Gougoussis, A. Kokalj, M. Lazzeri, L. Martin-Samos, N. Marzari, F. Mauri, R. Mazzarello, S. Paolini, A. Pasquarello, L. Paulatto, C. Sbraccia, S. Scandolo, G. Sclauzero, A. P. Seitsonen, A. Smogunov, P. Umari, and R. M. Wentzcovitch, http://stacks.iop.org/0953-8984/21/i=39/a=395502 J Phys-Condens Mat **21**, 395502 (2009).

[9] B. Grabowski, T. Hickel, and J. Neugebauer, "doibase-10.1103/PhysRevB.76.024309 Phys. Rev. B **76**, 024309 (2007).

[10] W. Li, L. Lindsay, D. A. Broido, D. A. Stewart, and N. Mingo, "doibase -10.1103/PhysRevB.86.174307 Phys Rev B **86**, 174307 (2012).

[11] K. D. Parrish, A. Jain, J. M. Larkin, W. A. Saidi, and A. J. H. McGaughey, -http://dx.doi.org/10.1103/PhysRevB.90.235201 Phys. Rev. B **90**, 235201 (2014).

[12] A. Dal Corso, S. Baroni, R. Resta, and S. de Gironcoli, "doibase -10.1103/PhysRevB.47.3588 Phys. Rev. B **47**, 3588 (1993).

[13] A. Jain and A. J. McGaughey, Computational Materials Science **110**, 115 (2015).

[14] J. Fabian and P. B. Allen, "doibase-10.1103/PhysRevLett.79.1885 Phys. Rev. Lett. **79**, 1885 (1997).

[15] P. B. Allen, "doibase-10.1103/PhysRevLett.59.1460 Phys. Rev. Lett. **59**, 1460 (1987).

[16] F. Giustino, M. L. Cohen, and S. G. Louie, "doibase-10.1103/PhysRevB.76.165108 Phys. Rev.

B **76**, 165108 (2007).

[17] G. Grimvall, *The electron-phonon interaction in metals*, Vol. 8 (North-Holland Amsterdam, 1981).